HHS Public Access

Author manuscript

FEBS J. Author manuscript; available in PMC 2018 November 01.

Published in final edited form as:

FEBS J. 2017 November ; 284(22): 3838–3848. doi:10.1111/febs.14271.

Understanding the Molecular Basis for Multiple Mitochondrial Dysfunctions Syndrome 1 (MMDS1): Impact of a Disease-Causing Gly189Arg Substitution on NFU1

Nathaniel A. Wesley[1], **Christine Wachnowsky**[1,2], **Insiya Fidai**[1,3], and **J. A. Cowan**[1,2,3,*]

[1]Department of Chemistry and Biochemistry, The Ohio State University, 100 West 18th Avenue, Columbus, Ohio 43210

[2]The Ohio State Biochemistry Program, The Ohio State University

[3]The Biophysics Graduate Program, The Ohio State University

Abstract

Iron-sulfur (Fe/S) cluster-containing proteins constitute one of the largest protein classes, with highly-varied function. Consequently, the biosynthesis of Fe/S clusters is evolutionarily conserved and mutations in intermediate Fe/S cluster scaffold proteins can cause disease, including multiple mitochondrial dysfunctions syndrome (MMDS). Herein, we have characterized the impact of defects occurring in the MMDS1 disease state that result from a point mutation (p.Gly189Arg) near the active site of NFU1, an iron-sulfur scaffold protein. *In vitro* investigation into the structure-function relationship of the Gly189Arg derivative, along with two other variants, reveals that substitution at position 189 triggers structural changes that increase flexibility, decrease stability, and alter the monomer-dimer equilibrium toward monomer, thereby impairing the ability of the Gly189X derivatives to receive an Fe/S cluster from physiologically-relevant sources.

Graphical Abstract

Proteins involved in iron-sulfur (Fe-S) cluster biosynthesis are critical for proper cellular function and homeostasis. In the Multiple Mitochondrial Dysfunctions Syndrome 1 (MMDS1) disease state, the Fe-S cluster protein NFU1 demonstrates a moderately severe G189R mutation that appears to primarily impact protein structure and oligomeric state and impairs the majority of cluster delivery pathways.

*Correspondence to: Dr. J. A. Cowan, Department of Chemistry and Biochemistry, The Ohio State University, 100 West 18th Avenue, Columbus, Ohio 43210. tel: 614-292-2703, cowan@chemistry.ohio-state.edu.

Author Contributions

NAW and CW conducted the experiments, analyzed the data, and wrote the manuscript. IF and JAC analyzed the data and wrote the manuscript.

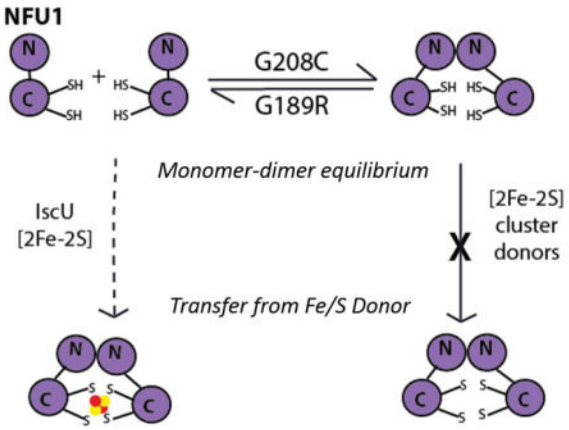

Keywords

Mitochondrial disease; iron-sulfur cluster; cluster exchange; protein stability; NFU1

Introduction

Characterization of novel proteins and their behavior in disease states has often aided in elucidation of their *in vivo* function. For example, an investigation of thiazolidinedione, a member of a class of drugs used to treat type 2 diabetes, led to discovery of a novel integral mitochondrial protein, mitoNEET that is now thought to have a key role in regulation of electron transfer and oxidative phosphorylation and potentially contributes to the etiology of the disease [10–12].

Similarly, a fatal mitochondrial disease, multiple mitochondrial dysfunctions syndrome 1 (MMDS1) has been shown to arise from point mutations in NFU1, an essential iron-sulfur (Fe/S) protein implicated in multiple metabolic pathways and in energy production through Fe/S cluster delivery and trafficking [13–19]. A number of recent studies have offered insight into the natural cellular roles of this protein by investigating the downstream Fe/S proteins affected by substitution of one disease-causing residue in close proximity to the cluster binding site (p.Gly208Cys) [15, 16, 18, 20]. The reduced function of target Fe/S proteins lipoic acid synthetase (LIAS) and succinate dehydrogenase (SDH) in the MMDS1 disease state suggests pathways that require proper function of the native NFU1 protein for cluster delivery [17, 21]. However, the precise function of NFU1 in humans remains unknown.

In previously documented MMDS1 patient cases, the disease was a result of a c.622G>T mutation (p.Gly208Cys), which was either homozygous, or heterozygous in conjunction with a deleterious frame-shift mutation (c.146delC null mutation). However, the heterozygous mutation alone was insufficient to display the disease phenotype, as the parents and siblings of the patients showed no symptoms [14, 15]. Analysis of the Gly208Cys NFU1 derivative by our laboratory revealed an altered monomer-dimer equilibrium *in vitro*, which prevented reconstitution from physiologically-relevant sources, suggesting the molecular basis for MMDS1 is the inability of NFU1 to accept cluster *in vivo*

[1]. Recently, a heterozygous p.Gly189Arg substitution in NFU1, present with either an additional mutation or the frameshift mutation, has been shown to impact metabolic pathways related to those affected by the Gly208Cys substitution, despite lying farther from the cluster binding site (Fig. 1) [20, 22, 23]. Interestingly, patients with this substitution experience milder symptoms and a later age of onset when compared with those with the homozygous Gly208Cys substitution form or the heterozygous Gly208Cys/c.146delC null mutation, suggesting a similar, yet less severe impairment of function. In order to understand the molecular basis for the milder MMDS1 phenotype of the Gly189Arg derivative and further elucidate the cellular role of NFU1, we have undertaken a detailed examination of the effects of amino acid substitution at position 189 on the structure and function of NFU1, in comparison to the previously documented native NFU1 and Gly208Cys variant [1].

Results and Discussion

Patient studies have reported a heterozygous genetic point mutation that converts a glycine at position 189 to an arginine (p.Gly189Arg), and when combined with either the previously discussed Gly208Cys substitution or a c.146delC null mutation, also results in the disease condition known as MMDS1, but generally with milder symptoms [18, 22]. Although position 189 is farther in sequence from the cluster-binding CXXC motif, the solution NMR structure of the C-terminal domain (PDB ID: 2M5O [24]) suggests that the glycine at position 189 lies in close proximity to the binding pocket (Fig. 1). Furthermore, the Gly189Arg substitution introduces a significantly larger and positively-charged side chain in place of a flexible, small aliphatic residue that could potentially affect the secondary Fe/S coordination sphere and thus Fe/S cluster transfer behavior, in addition to possible disruption of global protein structure. Given that the heterozygous Gly189Arg/Gly208Cys disease phenotype is less severe than the homozygous Gly208Cys or heterozygous Gly208Cys/c.146delC, yet still disease-causing, we sought to understand the molecular basis of the disease introduced by the Gly189Arg NFU1 substitution by introducing 3 different amino acid substitutions at this position (namely p.Gly189Arg, p.Gly189Lys, and p.Gly189Ala), particularly with regard to how such substitutions can disrupt protein structure and/or function.

Initial protein secondary structure characteristics were examined by circular dichroism (CD) spectroscopy to illustrate potential changes to the distribution of secondary structural elements. The values are summarized in Table 1 and demonstrate an overall increase in random coil with a corresponding loss of secondary structural elements, most noticeably in the Gly189Ala derivative. VTCD analysis shows that the overall increase in random coil could be attributed to increased flexibility in the molten globular C-terminal domain [25, 26], consistent with the lowered T_{m1} and ΔH_1 values, which most likely corresponds to the unfolding of the C-terminal domain, relative to the native (Fig. 2; Table 2) [1, 25]. However, the increase in random coil and decrease in α-helical content in the 189 variants relative to the native protein contrasts with increased T_{m2} values, which most likely corresponds to the unfolding of the N-terminal domain (Table 2). These results suggest that the 189 substitution introduces increased flexibility in the C-terminal domain, via a potentially destabilizing effect, that is then compensated by increased ordering in the N-terminal domain. All proteins

exhibited reversible melting on VTCD (data not shown), indicating that the overall protein folds are relatively stable.

Similar trends were observed in thermodynamic and structural characterization of Gly189X NFU1 by differential scanning calorimetry (DSC), which revealed significant destabilization of the C-terminal domain as reflected in T_{m1} and ΔH_{v1} values and a broadening of the peak corresponding to the C-terminal domain unfolding (Fig. 3; Tables 3 and 4). N-terminal domain melting temperatures (T_{m3}) are comparable to the native, although enthalpies of unfolding (ΔH_{v3}) are lower for the Gly189X derivatives, indicating that substitution has a global destabilizing effect (Table 3). Unlike the DSC characterization of the Gly208Cys derivative [1], only two melting events were observed in DSC for the 189 substitutions, most likely due to the high percentage of monomer (> 85%) as observed by analytical ultracentrifugation (Figs. 3 and 4; Table 5), whereas the native form displayed relatively equal monomer and dimer percentages, and Gly208Cys demonstrated preference for dimer. Together, these data indicate that substitution at position 189 increases the relative abundance of random coil, enhancing the flexibility of the C-terminal domain and marginally decreasing global stability, as evidenced by lowered melting temperatures and enthalpies of unfolding, to result in a high population of monomeric NFU1.

Given that substitution introduces small changes in thermodynamic parameters and noticeably affects oligomerization trends, we next sought to evaluate the effect of substitution on functional behavior relative to the native. Similar to the native and Gly208Cys variants [1], the Gly189 derivatives were capable of undergoing reconstitution *in vitro* through the use of $FeCl_3$ and L-cysteine with *Tm* NifS as a sulfide source. Following reconstitution, both UV and CD spectra were similar to those reported for the native and G208C forms [1], indicating the presence of a similarly bound [2Fe-2S] cluster. The cluster-bound 189 derivatives also form as a dimer around the Fe-S cluster, as confirmed by anaerobic AUC with monitoring at 420 nm (data not shown), with similar reconstitution yields to those observed for the native and Gly208Cys forms [1], which is functional for cluster transfer reactivity.

Our previous work with both native and Gly208Cys forms of NFU1 has shown that a glutathione-coordinated [2Fe-2S] cluster ($[2Fe\text{-}2S](GS)_4$) complex could be formed by Fe-S cluster extraction from reconstituted [2Fe-2S] cluster-bound native NFU1 and also Gly208Cys under conditions of excess GSH [1, 3]. Excess GSH is also able to extract the [2Fe-2S] cluster from NFU1 derivatives of residue 189 with at least fifteen-fold greater second-order rate constants for GSH extraction for Gly189X relative to the native and Gly208Cys variant (Fig. 5; Tables 6 and 7). The dramatic increase in Fe/S cluster lability *in vitro* observed for the Gly189Arg and Gly189Lys derivatives suggests that substitution, in addition to increasing flexibility of the C-terminal domain and preference for monomer, could simultaneously be promoting cluster reactivity through the introduction of charge or steric effects in the holo form.

As found for native and Gly208Cys human NFU1, [2Fe-2S] reconstituted G189X NFU1 could transfer cluster to ferredoxins 1 and 2 (Fdx1 and Fdx2) [3] and glutaredoxins 2 and 3 (Grx2 and Grx3) [5] (Fig. 6), as previously reported [3, 27–31]. In general, cluster transfer

from holo Gly189Ala was in line with the second-order rate constants for native NFU1, suggesting that the change from a glycine to an alanine has not perturbed this functional property (Table 7); though a protein-protein interaction may be disrupted for transfer to apo Grx2, as there is a slight decrease in the second-order rate constant for the transfer. For the Gly189Arg substitution, cluster transfer reactivity is only perturbed for transfer to Fdx1, which exhibits a three-fold larger second-order rate constant, and transfer to Grx2, which is slightly decreased, similar to Gly189Ala (Table 7). Interestingly, this substitution has not drastically impacted the ability to transfer cluster, other than an increased second-order rate constant in delivery to Fdx1, and increased lability in the presence of excess GSH. Cluster transfer from Gly189Lys was typically slower to downstream targets, except for transfer to apo Fdx2, where the second-order rate constant increased five-fold compared to native NFU1 (Table 7). Together, the kinetic data suggest that although transfer reactivity is not drastically affected, substitution at position 189 has the ability to tune cluster reactivity and affect *in vivo* cluster transfer properties for the reconstitution of downstream target or delivery proteins like LIAS and SDH.

However, although holo Gly189X NFU1 retained downstream cluster transfer reactivity, the cluster uptake properties of the 189 derivatives were significantly limited. Despite being largely monomeric, none of the 189 derivatives were able to accept cluster from the [2Fe-2S] $(GS)_4$ complex, though this has been shown to be a viable substrate for reconstitution of proteins such as native NFU1 and the mitochondrial export protein ABCB7 (Table 7) [1, 3, 31–33]. Likewise, the Gly189Arg and Gly189Lys derivatives were unable to receive an Fe/S cluster from the donor protein Isa1 (Table 7), a proposed Fe/S cluster scaffold protein, indicating that one putative *in vivo* reconstitution pathway could be interrupted in the Gly189Arg NFU1 MMDS1 disease state. Interestingly, the Gly189Ala construct was able to receive cluster from *S. pombe* Isa1, albeit at an impaired rate constant of 1200 ± 70 $M^{-1}min^{-1}$ reflecting the greater functional similarity between the native and Gly189Ala forms, also observed in the downstream cluster transfer rate constants (Table 7). However, in contrast to the Gly208Cys derivative, all 189 derivatives were able to accept cluster from human IscU, with transfer to Gly189Arg yielding a similar second-order rate constant to that of transfer to the native protein, though the Gly189Ala and Gly189Lys constructs demonstrated slightly slower uptake (Fig. 7; Table 7). In the heterozygous Gly189Arg/Gly208Cys MMDS1 disease state, reconstitution of NFU1 *in vivo* is most likely impaired due to the inability of the NFU1 derivative to receive an Fe-S cluster from the IscA1/2 assembly complex, yet not completely halted, due to the apparently viable IscU pathway for the Gly189Arg protein. The partially-functioning Fe/S trafficking pathway could explain the milder phenotype experienced by patients with the Gly189Arg substitution.

Our investigation into the Gly189Arg NFU1 substitution, as well as two other substitutions at position 189 has elucidated key facts regarding the structural and functional changes of NFU1 accompanying Gly189Arg substitution, and how these alterations could contribute to the MMDS1 phenotype. Substitution at 189 increases the random coil content, leading to an increase in flexibility and possible global protein destabilization, as evidenced by modestly decreased thermodynamic parameters, such as ΔH and T_m, for the C-terminal domain in particular. This change in structural characteristics significantly impacts the monomer-dimer equilibrium, though in the opposite direction from the previously characterized Gly208Cys

disease-causing substitution (Fig. 8), to promote monomer as the major species. As a result, substituted NFU1 has an impaired, although not eliminated ability to receive cluster from physiologically-relevant sources, and increased Fe/S cluster lability when present in near cellular concentrations of GSH. The relatively unaffected cluster transfer kinetics from NFU1 also suggest a problem with Fe/S cluster reconstitution or stability *in vivo* as opposed to an inability to transfer the cluster to downstream targets once bound, since transfer rates were relatively similar to the native protein. Together, these results are consistent with a milder phenotype, where substitution at 189 would still enable NFU1 function, albeit at reduced levels. Nevertheless, it remains unclear as to how NFU1 interacts with other potential target proteins in the MMDS1 disease state, such as LIAS and SDH, and the connection between NFU1 mutation and impaired interaction with these targets remains under investigation.

Materials and Methods

Protein preparation protocols

Stratagene QuikChange Mutagenesis was employed to introduce the p.Gly189Arg (c., p.Gly189Ala, and p.Gly189Lys point mutations into the full length human NFU1 gene in the pET28b(+) plasmid [1]. Mutant and wild-type constructs in BL21 DE3 cells were over-expressed in *E. coli*, and the proteins were purified using a TALON column as previously described [3]. A construct of human Grx2 (comprising residues 56–161), with a tobacco etch virus cleavable N-terminal His_6 tag in expression vector pNic-Bsa4, was kindly provided by Drs. Kavanagh, Muller-Knapp and Oppermann and protein was expressed and purified as previously reported [34]. *Schizosaccharomyces pombe* Isa1 protein was expressed and purified as previously reported [35]. Yeast Grx3 (Δ1–35) in pET28b(+) *E. coli* BL21 (DE3) was purified as noted [31]. Purification of *Hs* IscU and *Thermatoga maritima* (*Tm*) NifS was performed as previously reported [36–38]. Purified NFU1 constructs were reconstituted anaerobically with $FeCl_3$ and L-Cys as previously described, as were reconstitutions for Isa1 and IscU with $FeCl_3$ and Na_2S [1, 3]. Successful reconstitutions were confirmed by UV, CD and iron quantitation [39, 40].

The expression vector for human ferredoxin-1 (*Hs* Fdx1) was kindly provided by J. Markley and protein was expressed and purified according to literature procedures [41]. Purification for human ferredoxin-2 (*Hs* Fdx2) was performed as previously reported [42]. The ferredoxins purified as holo proteins and were subsequently converted to apo forms [3, 5].

Thermodynamic analyses and oligomeric state determination

Differential scanning calorimetry (DSC) was performed using a MicroCal VP-DSC (Malvern Instruments, Inc.) on 200 μM samples using a differential mode of 0.1 °C per minute from 10 °C to 100 °C, and analyzed using Origin software (Origin Labs) [1, 25]. For variable temperature circular dichroism (VTCD), 10 μM protein samples were dialyzed into 40 mM phosphate buffer, pH 7.4 for acquisition via a JASCO J-815 CD spectrometer with 0.1 cm quartz cells. Variable temperature studies were performed at a rate of 0.4 ° C min^{-1} from 20 to 95 °C monitoring signal at 222 nm, and data processed with Origin 7 (Origin Laboratories) to fit to equation 1 [1, 25]. Secondary structure prediction of 10 μM samples in

phosphate buffer (40 mM, pH 7.4) were obtained using CD by scanning from 300 – 165 nm. The resulting CD spectra were processed using the analysis program CDSSTR [7] using reference set 7 [43] found on the online server Dichroweb [8, 9]. Analytical ultracentrifugation (AUC) was employed to determine the oligomeric state of the NFU1 constructs. Apo proteins at 50 μM were monitored at 280 nm in the presence and absence of 1 mM TCEP, and the sedimentation profiles were fit to the Lamm equation using SEDFIT [2, 4].

Equation 1

VTCD data were fit to equation 1 for a three-state model indicative of a two-phase transition [25], where R is the ideal gas constant in calories per mole, T_m is the melting temperature in Kelvin, ΔH_V is the van't Hoff enthalpy, and ΔC_p is the change of heat capacity from folded to unfolded states. F and U represent the ellipticities (θ) of the folded and unfolded protein, respectively. It has been previously determined that the first observed transition can be assigned to the secondary structure transition of the melting C-terminal domain, and the second transition is indicative of the melting of the N-terminal domain [25]. The subscripts on T_m, ΔH_V, ΔC_p and U denote the transition parameters on the separate protein domains, with 1 for the C-terminal domain and 2 for the N-terminal domain.

$$\theta = \left\{ \exp\left[\left(\frac{1}{-RT}\right)\left(\Delta H_{V1}\left(1-\frac{T}{T_{m1}}\right)-\Delta C_{p1}\left((T_{m1}-T)+T\ln\frac{T}{T_{m1}}\right)\right)\right] / \left\{1 + \exp\left[\left(\frac{1}{-RT}\right)\left(\Delta H_{V1}\left(1-\frac{T}{T_{m1}}\right)-\Delta C_{p1}\left((T_{m1}-T)+T\ln\frac{T}{T_{m1}}\right)\right)\right]\right\}\right\}(F - U_1) + \left\{ \exp\left[\left(\frac{1}{-RT}\right)\left(\Delta H_{V2}\left(1-\frac{T}{T_{m2}}\right)-\Delta C_{p2}\left((T_{m2}-T)+T\ln\frac{T}{T_{m2}}\right)\right)\right] / \left\{1 + \exp\left[\left(\frac{1}{-RT}\right)\left(\Delta H_{V2}\left(1-\frac{T}{T_{m2}}\right)-\Delta C_{p2}\left((T_{m2}-T)+T\ln\frac{T}{T_{m2}}\right)\right)\right]\right\}\right\}(U_1 - U_2) + U_2$$

Kinetic analysis for second-order rate constant determination

Kinetic cluster transfer experiments were performed by use of CD and were based on the cluster transfer experiments by Johnson and coworkers [44, 45], and refined by our own group [3, 31]. All cluster transfer experiments were carried out on a JASCO J-815 CD spectrometer with a 1 cm anaerobic quartz cuvette by scanning from 600 – 300 nm at 200 nm/min and 25 °C after introduction of the degassed holo protein or degassed glutathione-complexed [2Fe-2S] cluster ($[2Fe\text{-}2S](GS)_4$) complex. CD data were converted to the percentage of cluster transferred based on the concentration of [2Fe-2S] cluster and fit by

use of DynaFit [27] to determine the second-order rate constants by best-fit simulation to second-order kinetics [5, 6].

Cluster extraction from holo NFU1 constructs was performed by UV-Visible spectrophotometry by scanning from 800 - 200 nm at 600 nm/min and 25°C after the addition of holo protein. Glutathione concentrations were varied from 0.2 – 2 mM, and the reaction course monitored via the change in absorbance at 420 nm. The k_{obs} was plotted against GSH concentration and fit to equation 2 to obtain the apparent K and first-order rate constant [3, 31]. The first-order rate constant was divided by K to determine the second-order rate constant.

Equation 2

The plot of k_{obs} versus the concentration of GSH for cluster extraction was fit to a saturation kinetics model [31]. The values obtained from the fit were utilized to calculate the overall second-order rate constant.

$$k_{obs} = \frac{k_1}{1 + \frac{K}{[GSH]}}$$

Acknowledgments

We thank Dr. Marina Bakhtina for her assistance with analytical ultracentrifugation experiments and Dr. Tom Magliery for providing a thermocycler. This work was supported by a grant from the National Institutes of Health [AI072443]. Nathaniel Wesley was supported by scholarships from the Ohio State Undergraduate Research Office and the Honors College of Arts and Sciences. Christine Wachnowsky was supported by an NIH Chemistry/Biology Interface training grant (T32 GM095450), as well an Ohio State University Presidential Fellowship.

Abbreviations

MMDS1	Multiple Mitochondrial Dysfunctions Syndrome 1
GSH	Glutathione
DSC	Differential Scanning Calorimetry
VTCD	Variable Temperature Circular Dichroism
ESI-MS	Electrospray Ionization Mass Spectrometry
CD	Circular Dichroism
AUC	Analytical Ultracentrifugation
IscU	Iron-sulfur cluster scaffold protein
Isa1	Iron-sulfur cluster assembly protein
Fdx	Ferredoxin
Grx	Glutaredoxin
LIAS	Lipoate synthase

References

1. Wachnowsky C, Wesley NA, Fidai I, Cowan JA. Understanding the molecular basis for Multiple Mitochondrial Dysfunctions Syndrome 1 (MMDS1) - Impact of a disease-causing Gly208Cys substitution on structure and activity of NFU1 in the Fe/S cluster biosynthetic pathway. J Mol Biol. 2017; 429:790–807. [PubMed: 28161430]
2. Lamm O. Die Differentialgleichung der Ultrazentrifugierung. Ark Mat Astr Fys. 1929:1–4.
3. Wachnowsky C, Fidai I, Cowan JA. Iron-sulfur cluster exchange reactions mediated by the human Nfu protein. J Biol Inorg Chem. 2016; 21:825–836. [PubMed: 27538573]
4. Schuck P. Size-distribution analysis of macromolecules by sedimentation velocity ultracentrifugation and Lamm equation modeling. Biophys J. 2000; 78:1606–1619. [PubMed: 10692345]
5. Fidai I, Wachnowsky C, Cowan JA. Mapping cellular Fe–S cluster uptake and exchange reactions – divergent pathways for iron–sulfur cluster delivery to human ferredoxins. Metallomics. 2016; 8:1283–1293. [PubMed: 27878189]
6. Wachnowsky C, Fidai I, Cowan JA. Cytosolic iron-sulfur cluster transfer: a proposed kinetic pathway for the reconstitution of glutaredoxin 3. FEBS Lett. 2016; 590:4531–4540. [PubMed: 27859051]
7. Sreerama N, Woody RW. Estimation of protein secondary structure from CD spectra: Comparison of CONTIN, SELCON and CDSSTR methods with an expanded reference set. Anal Chem. 2000; 287:252–260.
8. Whitmore L, Wallace BA. DICHROWEB, an online server for protein secondary structure analyses from circular dichroism spectroscopic data. Nucleic Acids Res. 2004; 32:W668–W673. [PubMed: 15215473]
9. Whitmore L, Wallace BA. Protein secondary structure analyses from circular dichroism spectroscopy: Methods and reference databases. Biopolymers. 2008; 89:392–400. [PubMed: 17896349]
10. Colca JR, McDonald WG, Waldon DJ, Leone JW, Lull JM, Bannow CA, Lund ET, Mathews WR. Identification of a novel mitochondrial protein (“mitoNEET”) cross-linked specifically by a thiazolidinedione photoprobe. Am J Physiol Endocrinol Metab. 2004; 286:E252–E260. [PubMed: 14570702]
11. Wiley SE, Murphy AN, Ross SA, van der Geer P, Dixon JE. MitoNEET is an iron-containing outer mitochondrial membrane protein that regulates oxidative capacity. Proceedings of the National Academy of Sciences. 2007; 104:5318–5323.
12. Fernández-Real JM, López-Bermejo A, Ricart W. Cross-talk between iron metabolism and diabetes. Diabetes. 2002; 51:2348–2354. [PubMed: 12145144]
13. Seyda A, Newbold RF, Hudson TJ, Verner A, MacKay N, Winter S, Feigenbaum A, Malaney S, Gonzalez-Halphen D, Cuthbert AP, et al. A Novel Syndrome Affecting Multiple Mitochondrial Functions, Located by Microcell-Mediated Transfer to Chromosome 2p14–2p13. Am J Hum Genet. 2001; 68:386–396. [PubMed: 11156534]
14. Cameron JM, Janer A, Levandovskiy V, Mackay N, Rouault TA, Tong WH, Ogilvie I, Shoubridge EA, Robinson BH. Mutations in iron-sulfur cluster scaffold genes NFU1 and BOLA3 cause a fatal deficiency of multiple respiratory chain and 2-oxoacid dehydrogenase enzymes. Am J Hum Genet. 2011; 89:486–495. [PubMed: 21944046]
15. Navarro-Sastre A, Tort F, Stehling O, Uzarska Marta A, Arranz José A, del Toro M, Labayru MT, Landa J, Font A, Garcia-Villoria J, et al. A fatal mitochondrial disease is associated with defective NFU1 function in the maturation of a subset of mitochondrial Fe-S proteins. Am J Hum Genet. 2011; 89:656–667. [PubMed: 22077971]
16. Ferrer-Cortès X, Font A, Bujan N, Navarro-Sastre A, Matalonga L, Arranz JA, Riudor E, del Toro M, Garcia-Cazorla A, Campistol J, et al. Protein expression profiles in patients carrying NFU1 mutations. Contribution to the pathophysiology of the disease. J Inherit Metab Dis. 2012; 36:841–847. [PubMed: 23179554]
17. Stehling O, Wilbrecht C, Lill R. Mitochondrial iron–sulfur protein biogenesis and human disease. Biochimie. 2014; 100:61–77. [PubMed: 24462711]

18. Nizon M, Boutron A, Boddaert N, Slama A, Delpech H, Sardet C, Brassier A, Habarou F, Delahodde A, Correia I, et al. Leukoencephalopathy with cysts and hyperglycinemia may result from NFU1 deficiency. Mitochondrion. 2014; 15:59–64. [PubMed: 24462778]
19. Ferrer-Cortès X, Narbona J, Bujan N, Matalonga L, Del Toro M, Arranz JA, Riudor E, Garcia-Cazorla A, Jou C, O'Callaghan M, et al. A leaky splicing mutation in NFU1 is associated with a particular biochemical phenotype. Consequences for the diagnosis. Mitochondrion. 2016; 26:72–80. [PubMed: 26688339]
20. Ahting U, Mayr JA, Vanlander AV, Hardy SA, Santra S, Makowski C, Alston CL, Zimmermann FA, Abela L, Plecko B, et al. Clinical, biochemical, and genetic spectrum of seven patients with NFU1 deficiency. Front Genet. 2015:06.
21. Maio N, Rouault TA. Iron–sulfur cluster biogenesis in mammalian cells: New insights into the molecular mechanisms of cluster delivery. Biochim Biophys Acta. 2015; 1853:1493–1512. [PubMed: 25245479]
22. Tonduti D, Dorboz I, Imbard A, Slama A, Boutron A, Pichard S, Elmaleh M, Vallée L, Benoist J, Ogier H, et al. New spastic paraplegia phenotype associated to mutation of NFU1. Orphanet J Rare Dis. 2015; 10:13. [PubMed: 25758857]
23. Invernizzi F, Ardissone A, Lamantea E, Garavaglia B, Zeviani M, Farina L, Ghezzi D, Moroni I. Cavitating leukoencephalopathy with multiple mitochondrial dysfunction syndrome and NFU1 mutations. Front Genet. 2014:5. [PubMed: 24523726]
24. Cai K, Liu G, Frederick Ronnie O, Xiao R, Montelione Gaetano T, Markley John L. Structural/functional properties of human NFU1, an intermediate [4Fe-4S] carrier in human mitochondrial iron-sulfur cluster biogenesis. Structure. 2016; 24:2080–2091. [PubMed: 27818104]
25. Li J, Ding S, Cowan JA. Thermodynamic and structural analysis of human NFU conformational chemistry. Biochemistry. 2013; 52:4904–4913. [PubMed: 23796308]
26. Liu Y, Cowan JA. Iron–sulfur cluster biosynthesis: characterization of a molten globule domain in human NFU. Biochemistry. 2009; 48:7512–7518. [PubMed: 19722697]
27. Kuzmic P. Program DYNAFIT for the analysis of enzyme kinetic data: Application to HIV proteinase. Anal Biochem. 1996; 237:260–273. [PubMed: 8660575]
28. Gao H, Subramanian S, Couturier J, Naik SG, Kim S-K, Leustek T, Knaff DB, Wu H-C, Vignols F, Huynh BH, et al. *Arabidopsis thaliana* Nfu2 accommodates [2Fe-2S] or [4Fe-4S] clusters and is competent for *in vitro* maturation of chloroplast [2Fe-2S] and [4Fe-4S] cluster-containing proteins. Biochemistry. 2013; 52:6633–6645. [PubMed: 24032747]
29. Stephens PJ, Thomson AJ, Dunn JBR, Keiderling TA, Rawlings J, Rao KK, Hall DO. Circular Dichroism and Magnetic Circular Dichroism of Iron-Sulfur Proteins. Biochemistry. 1978; 22:4770–4778.
30. Mapolelo DT, Zhang B, Randeniya S, Albetel AN, Li H, Couturier J, Outten CE, Rouhier N, Johnson MK. Monothiol glutaredoxins and A-type proteins: partners in Fe-S cluster trafficking. Dalton Trans. 2013; 42:3107–3115. [PubMed: 23292141]
31. Fidai I, Wachnowsky C, Cowan JA. Glutathione-complexed [2Fe-2S] clusters function in Fe-S cluster storage and trafficking. J Biol Inorg Chem. 2016; 21:887–901. [PubMed: 27590019]
32. Qi W, Li J, Chain CY, Pasquevich GA, Pasquevich AF, Cowan JA. Glutathione Complexed Fe–S Centers. J Am Chem Soc. 2012; 134:10745–10748. [PubMed: 22687047]
33. Qi W, Li J, Cowan JA. A structural model for glutathione-complexed iron–sulfur cluster as a substrate for ABCB7-type transporters. Chem Commun. 2014; 50:3795.
34. Qi W, Cowan JA. Mechanism of glutaredoxin-ISU [2Fe-2S] cluster exchange. Chem Commun. 2011; 47:4989–4991.
35. Wu G, Mansy SS, Hemann C, Hille R, Surerus KK, Cowan JA. Iron-sulfur cluster biosynthesis: characterization of *Schizosaccharomyces pombe* Isa1. J Biol Inorg Chem. 2002; 7:526–532. [PubMed: 11941510]
36. Foster MW, Mansy SS, Hwang J, Penner-Hahn JE, Surerus KK, Cowan JA. A mutant human IscU protein contains a stable $[2Fe\text{-}2S]^{2+}$ center of possible functional significance. J Am Chem Soc. 2000; 122:6805–6806.

37. Mansy SS, Xiong Y, Hemann C, Hille R, Sundaralingam M, Cowan JA. Crystal structure and stability studies of C77S HiPIP: a serine ligated [4Fe-4S] cluster. Biochemistry. 2002; 41:1195–1201. [PubMed: 11802718]

38. Nuth M, Yoon T, Cowan JA. Iron-sulfur cluster biosynthesis: characterization of iron nucleation sites for assembly of the $[2Fe\text{-}2S]^{2+}$ cluster core in IscU proteins. J Am Chem Soc. 2002; 124:8774–8775. [PubMed: 12137512]

39. Moulis J-M, Meyer J. Characterization of the selenium-substituted 2[4Fe-4Se] ferredoxin from *Clostridium pasteurianum*. Biochemistry. 1982; 21:4762–4771. [PubMed: 6753926]

40. Wu, S-p, Wu, G., Surerus, KK., Cowan, JA. Iron-sulfur cluster biosynthesis. Kinetic analysis of [2Fe-2S] cluster transfer from holo ISU to apo Fd: role of redox chemistry and a conserved aspartate. Biochemistry. 2002; 41:8876–8885. [PubMed: 12102630]

41. Xia B, Cheng H, Bandarian V, Reed GH, Markley JL. Human ferredoxin: overproduction in *Escherichia coli*, reconstitution *in vitro*, and spectroscopic studies of iron-sulfur cluster ligand cysteine-to-serine mutants. Biochemistry. 1996; 35:9488–9495. [PubMed: 8755728]

42. Qi W, Li J, Cowan JA. Human ferredoxin-2 displays a unique conformational change. Dalton Trans. 2013; 42:3088–3091. [PubMed: 23208207]

43. Janes, RW. Reference Datasets Circular Dichroism and Synchrotron Radiation Circular Dichroism Spectroscopy of Proteins. In: Wallace, BA., Janes, RW., editors. Modern Techniques in Circular Dichroism and Synchrotron Radiation Circular Dichroism Spectroscopy. IOS Press; Amsterdam: 2008.

44. Mapolelo DT, Zhang B, Randeniya S, Albetel A-N, Li H, Couturier J, Outten CE, Rouhier N, Johnson MK. Monothiol glutaredoxins and A-type proteins: partners in Fe–S cluster trafficking. Dalton Trans. 2013; 42:3107. [PubMed: 23292141]

45. Shakamuri P, Zhang B, Johnson MK. Monothiol glutaredoxins function in storing and transporting [2Fe-2S] clusters assembled on IscU scaffold proteins. J Am Chem Soc. 2012; 134:15213–15216. [PubMed: 22963613]

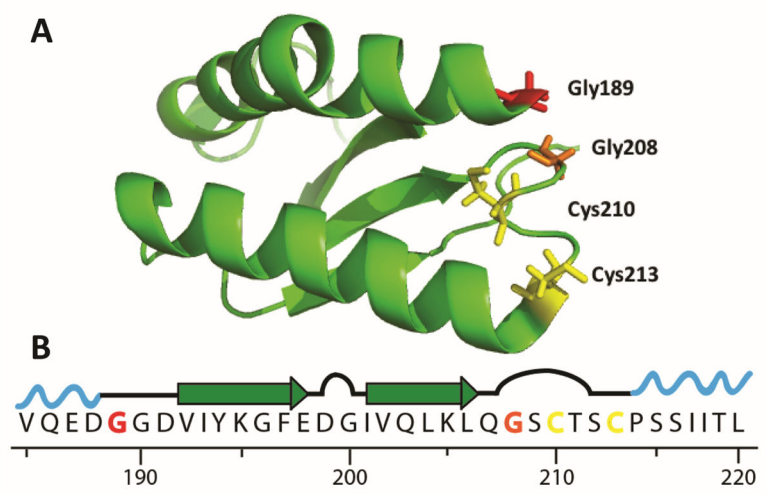

Figure 1.

(**A**) Solution NMR structure of the C-terminal domain of the human NFU1 protein (PDB ID: 2M5O) with corresponding cluster ligating cysteines in yellow and the glycine at position 189 in red. Although only the C-terminal domain is shown, numbering corresponds to the positions in the full length protein. (**B**) Sequence chain view to illustrate the residues near the glycine at position 189. The coloring scheme matches part (**A**). The glycine at position 208 that is also implicated in MMDS1 is colored orange.

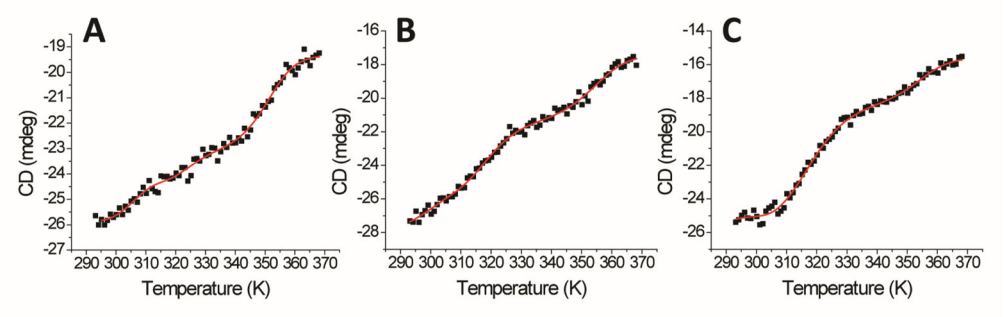

Figure 2.

VTCD trace for the melting of (**A**) 10 μM Gly189Arg, (**B**) Gly189Ala and (**C**) Gly189Lys human NFU1 in 40 mM phosphate, pH 7.4. Data were fit to a two-phase model (Eq. 1) to obtain T_m and ΔH_V, which are shown in Table 2. CD units of ellipticity (mdeg) were used directly without conversion to molar ellipticity, because the van't Hoff enthalpies are independent of such a factor [25].

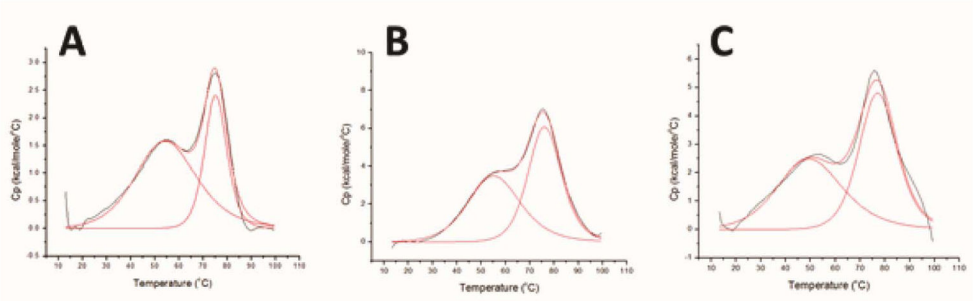

Figure 3.

Differential scanning calorimetry profiles for (**A**) 0.2 mM Gly189Arg, (**B**) 0.2 mM Gly189Ala, and (**C**) 0.15 mM Gly189Lys human NFU1. The protein was in 50 mM HEPES, 100 mM NaCl, and pH 7.4. The data were fit using Origin 7.0 to obtain the T_m and ΔH_V values listed in Tables 3 and 4.

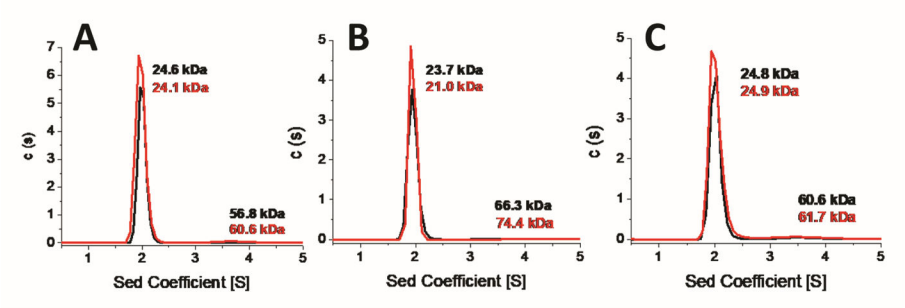

Figure 4.

AUC profile for (**A**) apo Gly189Arg, (**B**) Gly189Ala, and (**C**) Gly189Lys NFU1. Apo protein was sedimented in the absence of TCEP (black) and in the presence of 1 mM TCEP (red). Sedimentation was monitored at 280 nm. The AUC results were fit to the Lamm equation [2, 4] using a continuous distribution model to obtain the peaks and molecular weights shown above. The peak percentages are listed in Table 5.

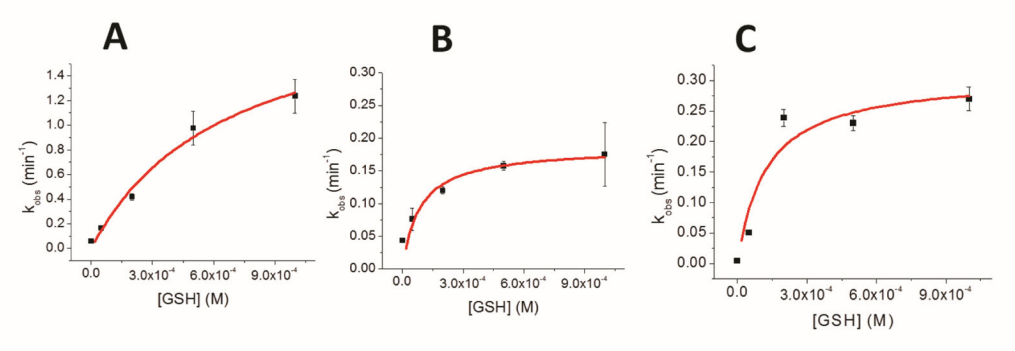

Figure 5.

GSH extraction of the [2Fe-2S] cluster from holo (**A**) 10 μM Gly189Arg NFU1, (**B**) 10 μM Gly189Ala NFU1, and (**C**) 10 μM Gly189Lys NFU1, to form the [2Fe-2S](GS)$_4$ complex. The change in absorbance at 420 nm was monitored over the course of one hour. The change in absorbance at 420 nm was plotted against time for each of the different concentrations of GSH and fit to an exponential to obtain the k_{obs} for each concentration. k_{obs} data was plotted against GSH concentration and fit to equation 2 to determine an apparent dissociation constant K and a first-order rate constant k_1 for formation of the [2Fe-2S](GS)$_4$ complex (Table 6). k_1 was divided by K to determine an overall second-order rate constant of 4400 ± 630 $M^{-1}min^{-1}$ for (**A**), 2000 ± 330 $M^{-1}min^{-1}$ for (**B**), and 2590 ± 420 $M^{-1}min^{-1}$ for (**C**) [31]. Error bars are defined as ± SD, with n=3.

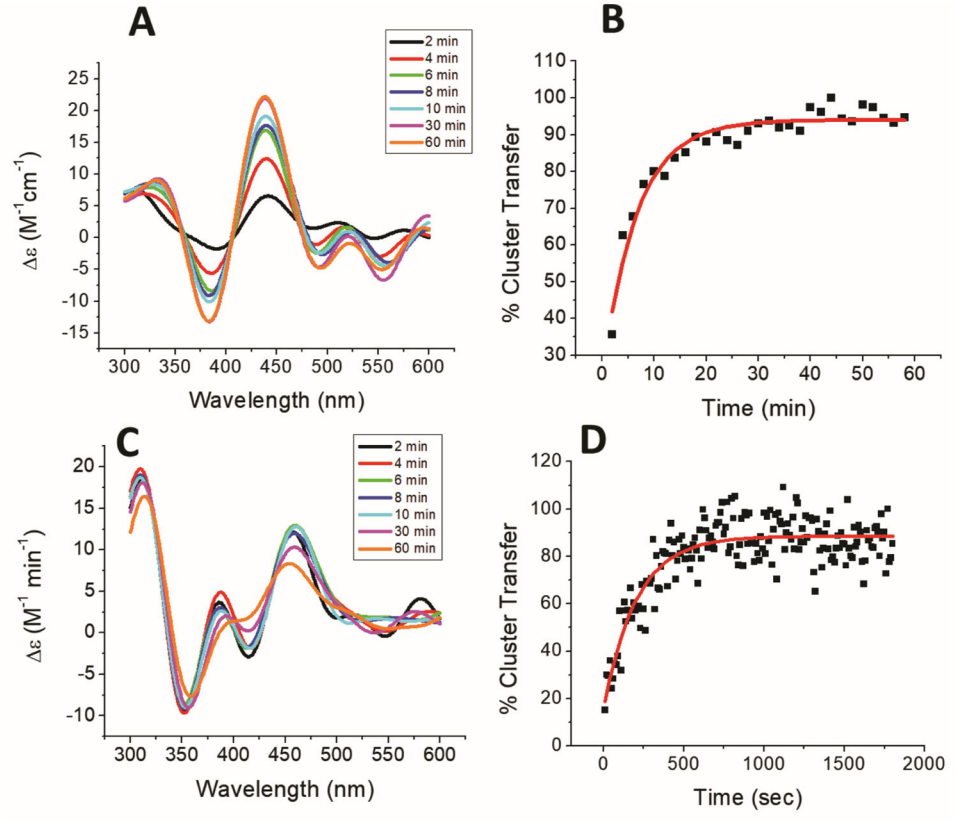

Figure 6.

Representative [2Fe-2S] kinetic cluster transfer reactions. (**A**) Time course of cluster transfer from holo reconstituted human Gly189Arg NFU1 to apo human ferredoxin 1 (Fdx1). Time course for cluster transfer to Fdx1 monitored by CD in 50 mM HEPES and 100 mM NaCl (pH 7.5). Spectra were recorded every 2 min after the addition of holo Gly189Arg NFU1 and were converted to percent cluster transfer (**B**) to yield an apparent second-order rate constant from DynaFit of 12,500 ± 1000 M−1 min−1 based on the concentration of the [2Fe-2S] cluster [27]. (**C**) Time course of [2Fe-2S] cluster transfer from holo reconstituted human Gly189Arg NFU1 to apo *S. cerevisiae* glutaredoxin 3 (Grx3) monitored by CD in 50 mM HEPES and 100 mM NaCl (pH 7.5). Spectra were recorded every 2 min after the addition of holo Gly189Arg NFU1. However transfer was too rapid to monitor, so cluster transfer was monitored from 465-455 nm every 10 sec and converted to percent cluster transfer (**D**) to determine an apparent second-order rate constant using DynaFit of 39,500 ± 8000 M^{-1} min^{-1} based on the concentration of the [2Fe-2S] cluster [27].

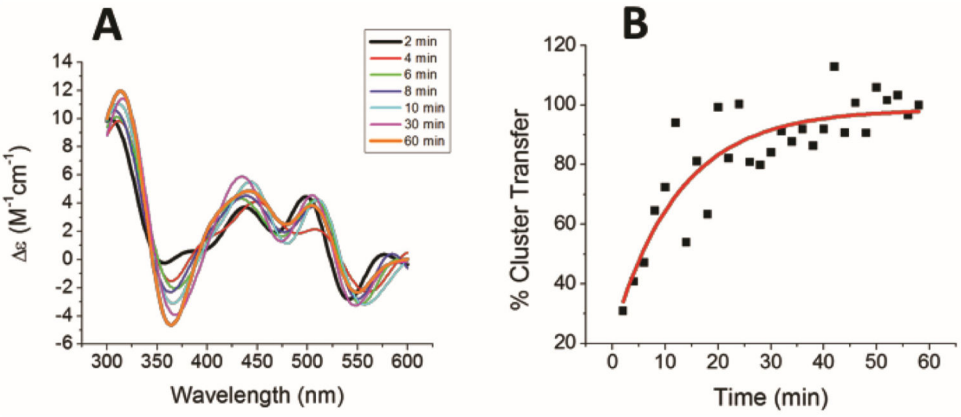

Figure 7.

Representative cluster transfer reaction for delivery of a [2Fe-2S] cluster into Nfu from a physiologically relevant donor. Kinetics of [2Fe-2S] cluster transfer from holo reconstituted human IscU to human Gly189Arg NFU1. (**A**) Time course for cluster transfer to human Gly189Arg NFU1 monitored by CD in 50 mM HEPES and 100 mM NaCl (pH 7.5). Spectra were recorded every 2 min following addition of holo IscU and were converted to (**B**) percent cluster transfer to yield an apparent second-order rate constant from DynaFit of 5700 ± 1400 M−1 min−1 based on the concentration of the [2Fe-2S] cluster [27].

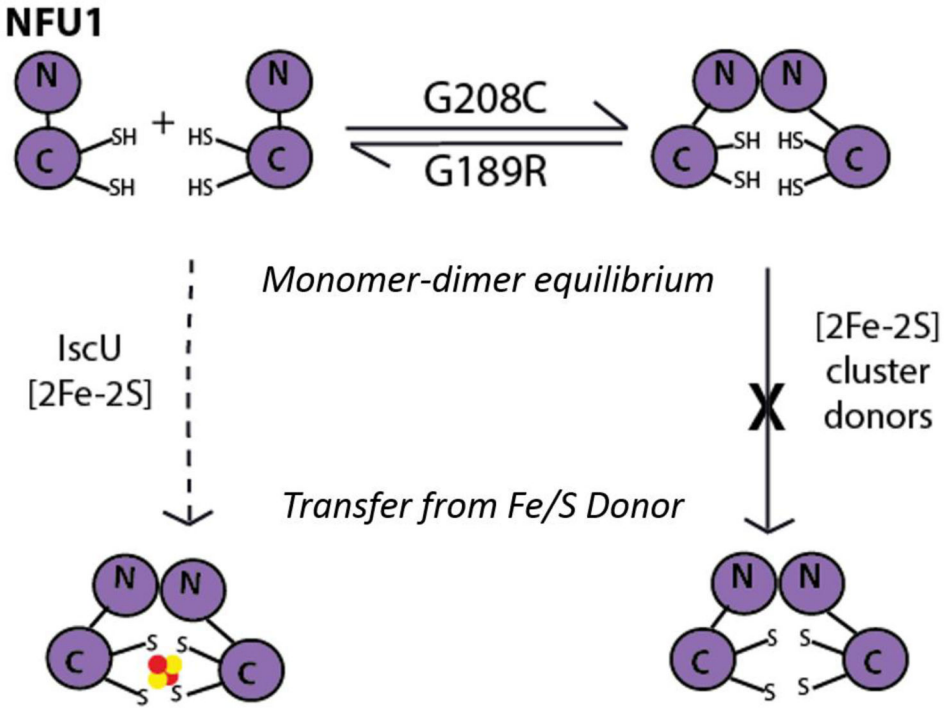

Figure 8.

A schematic illustration, highlighting the distinct impact of Gly189Arg and Gly208Cys substitutions on the NFU1 monomer-dimer equilibrium and uptake of [2Fe-2S] cluster to form holo dimer. The Gly208Cys derivative is incapable of receiving cluster from any source [1], while Gly189Arg accepts cluster from IscU.

Table 1

Percentages of secondary structural elements measured by CD and analyzed using the analysis program CDSSTR [7] on the online Dichroweb server [3, 8, 9].

	α-helix	β-sheet	random coil
native NFU1	47 %	21 %	33 %
Gly189Arg NFU1	37 %	19 %	44 %
Gly189Ala NFU1	23 %	20 %	57 %
Gly189Lys NFU1	40 %	17 %	44 %

Table 2

Native NFU1 and Gly189X NFU1 at 10 μM were subjected to melting from 20 to 95 °C at 0.4 °C per min as shown in Fig. 2. Table 2 shows the data fit to a three-phase melting process from fitting with equation 1.

	T_{m1} (°C)	ΔH_{v1} (kcal/mol)	T_{m2} (°C)	ΔH_{v2} (kcal/mol)
native NFU1	55 ± 3	33 ± 2	74 ± 2	36 ± 3
Gly189Arg NFU1	38 ± 1	16 ± 1	79 ± 2	34 ± 4
Gly189Ala NFU1	40 ± 3	21 ± 1	80 ± 3	32 ± 1
Gly189Lys NFU1	42 ± 4	24 ± 4	77 ± 2	40 ± 1

Table 3

Melting temperatures as determined from fits to the DSC data. The DSC profiles used for fitting are shown in Fig. 3. Native and Gly208Cys data were previously reported [1].

	T_{m1} (°C)	T_{m2} (°C)	T_{m3} (°C)
native NFU1	60 ± 1	--	73 ± 1
Gly208Cys NFU1	49 ± 6	64 ± 2	74 ± 4
Gly189Arg NFU1	52 ± 5	--	75 ± 1
Gly189Ala NFU1	53 ± 3	--	77 ± 1
Gly189Lys NFU1	49 ± 2	--	80 ± 4

Table 4

Enthalpies of melting determined by DSC. The DSC profiles used for data fitting are shown in Fig. 3. Native and Gly208Cys data were previously reported [1].

	ΔH_{v1} (kcal/mol)	ΔH_{v2} (kcal/mol)	ΔH_{v3} (kcal/mol)
native NFU1	41 ± 2	--	74 ± 5
Gly208Cys NFU1	33 ± 4	50 ± 2	74 ± 4
Gly189Arg NFU1	24 ± 1	--	65 ± 20
Gly189Ala NFU1	29 ± 2	--	55 ± 3
Gly189Lys NFU1	28 ± 6	--	44 ± 6

Table 5

Analytical ultracentrifugation results of the NFU1 derivatives in the presence and absence of 1 mM TCEP, as shown in Fig. 4. The obtained molecular weights were classified according to the most likely corresponding oligomeric state [1–4].

	Monomer	With TCEP	Dimer	With TCEP	Tetramer	With TCEP
Native	45 %	44 %	52 %	44 %	--	--
Gly208Cys	29 %	30 %	58 %	60 %	6 %	1.5 %
Gly189Arg	95 %	94 %	4 %	4%	--	--
Gly189Ala	95 %	95 %	3 %	3 %	--	--
Gly189Lys	93 %	89 %	5 %	6 %	--	--

Table 6

Apparent dissociation constants K for the pre-reaction complex of holo protein and GSH and first-order rate constants k_1 for formation of the [2Fe-2S](GS)$_4$ complex during cluster extraction from holo proteins by free glutathione as determined from equation 2. Overall second-order rate constants for cluster extraction were determined by dividing k_1 by K. The values are shown in Table 7.

Construct	K (M)	k_1 (min^{-1})
G189R	0.00032	1.4
G189A	0.00009	0.18
G189K	0.00012	0.31

Table 7

Second-order rate constants for [2Fe-2S] cluster transfer to and from NFU1. Native and Gly208Cys transfer rate constants were previously determined using the same CD or UV method [1, 3, 5, 6]. All values have units of M^{-1} min^{-1}.

	native	Gly208Cys	Gly189Arg	Gly189Ala	Gly189Lys
human NFU1 to human Fdx1	4700 ± 800	2600 ± 300	12500 ± 1000	3300 ± 750	2500 ± 930
human NFU1 to human Fdx2	3900 ± 1200	1200 ± 200	3100 ± 250	3400 ± 200	21000 ± 2900
human NFU1 to human Grx2	3740 ± 77	22400 ± 5000	2700 ± 770	1500 ± 500	2100 ± 300
human NFU1 to *S. cerevisiae* Grx3	36200 ± 7700	14500 ± 3500	39500 ± 8000	29000 ± 3700	6700 ± 1900
human IscU to Human NFU1	4750 ± 8	no transfer	5000 ± 1200	3200 ± 30	3000 ± 110
S. pombe Isa to human NFU1	6700 ± 1560	no transfer	no transfer	1750 ± 110	no transfer
[2Fe-2S](GS)$_4$to human NFU1	1930 ± 210	no transfer	no transfer	no transfer	no transfer
human NFU1 to [2Fe-2S](GS)$_4$	130 ± 22	140 ± 20	4400 ± 630	2000 ± 330	2590 ± 420